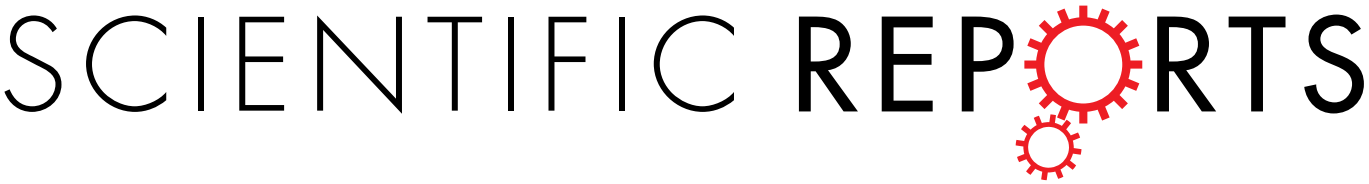

OPEN

TiO_xN_y Modified TiO_2 Powders Prepared by Plasma Enhanced Atomic Layer Deposition for Highly Visible Light Photocatalysis

Received: 11 April 2018
Accepted: 30 July 2018
Published online: 14 August 2018

Yan-Qiang Cao, Xi-Rui Zhao, Jun Chen, Wei Zhang, Min Li, Lin Zhu, Xue-Jin Zhang, Di Wu & Ai-Dong Li

In this work, TiN film deposited by plasma enhanced atomic layer deposition (PEALD) is adopted to modify the commercial anatase TiO_2 powders. A series of analyses indicate that the surface modification of 20, 50 and 100 cycles of TiN by PEALD does not change the morphology, crystal size, lattice parameters, and surface area of TiO_2 nano powders, but forms an ultrathin amorphous layer of nitrogen doped TiO_2 (TiO_xN_y) on the powder surfaces. This ultrathin TiO_xN_y can facilitate the absorption of TiO_2 in visible light spectrum. As a result, TiO_xN_y coated TiO_2 powders exhibit excellent photocatalytic degradation towards methyl orange under the visible light with good photocatalytic stability compared to pristine TiO_2 powders. TiO_xN_y (100 cycles PEALD TiN) coated TiO_2 powders exhibit the excellent photocatalytic activity with the degradation efficiency of 96.5% in 2 hours, much higher than that of pristine TiO_2 powder of only 4.4%. These results clearly demonstrate that only an ultrathin surface modification layer can dramatically improve the visible light photocatalytic activity of commercial TiO_2 powders. Therefore, this surface modification using ALD is an extremely promising route to prepare visible light active photocatalysts.

Titanium dioxide (TiO_2) is the most widely investigated photocatalyst due to its good photocatalytic activity, high chemical and thermal stability, nontoxicity, low cost, and excellent degradation capacity[1–3]. However, a large band gap (3.2 eV) of TiO_2 has limited its practical applications since it can be only activated by the illumination of ultra-violet light, which only makes up 4–5% of the solar spectrum[4]. In order to utilize a wider solar spectrum, it is highly desirable that the TiO_2-based photocatalysts can work under visible light. Therefore, considerable efforts have been devoted for TiO_2 to facilitate its visible light absorption. There are several ways can be applied to achieve this goal, such as element doping[5–7] and coupling with metal or other semiconductors[8–11]. Among various approaches, non-metal doping of TiO_2 has shown great promise in enhancing visible light active photocatalysis, with nitrogen doping being the most promising dopant[3,12,13]. N-doped TiO_2 nanomaterials have been synthesized successfully by various methods, such as hydrolysis of TTIP in a water/amine mixture, post-treatment of the TiO_2 sol with amines, ball milling of TiO_2 in a NH_3 water solution[14–16]. N-doped TiO_2 nanomaterials could also be obtained by annealing TiO_2 under NH_3 flux at high temperature[17]. In addition, several film deposition techniques including sputtering[18], chemical vapour deposition[19], atomic layer deposition (ALD)[20], have also been applied to prepare N-doped TiO_2 film. The visible light photocatalytic activity of N-doped TiO_2 nanomaterials has been explored thoroughly. Although the effect of N doping on photocatalytic enhancement of TiO_2 is still debated, it is well accepted that N doping can cause the red shift absorption threshold of TiO_2, improving the visible light photocatalytic activity[21,22].

ALD is a novel and promising thin film deposition technique based on sequential self-limited and complementary surface chemisorption reactions, which is able to deposit ultrathin, uniform, and conformal layers, and it's especially suitable for coating 3D complex structures. In recent years, ALD has attracted increasing attention in synthesis and surface engineering of complex nanostructures in recent years[23–26]. ALD has shown great

National Laboratory of Solid State Microstructures and Department of Materials Science and Engineering, College of Engineering and Applied Sciences, Collaborative Innovation Center of Advanced Microstructures, Nanjing University, Nanjing, 210093, People's Republic of China. Correspondence and requests for materials should be addressed to A.-D.L. (email: adli@nju.edu.cn)

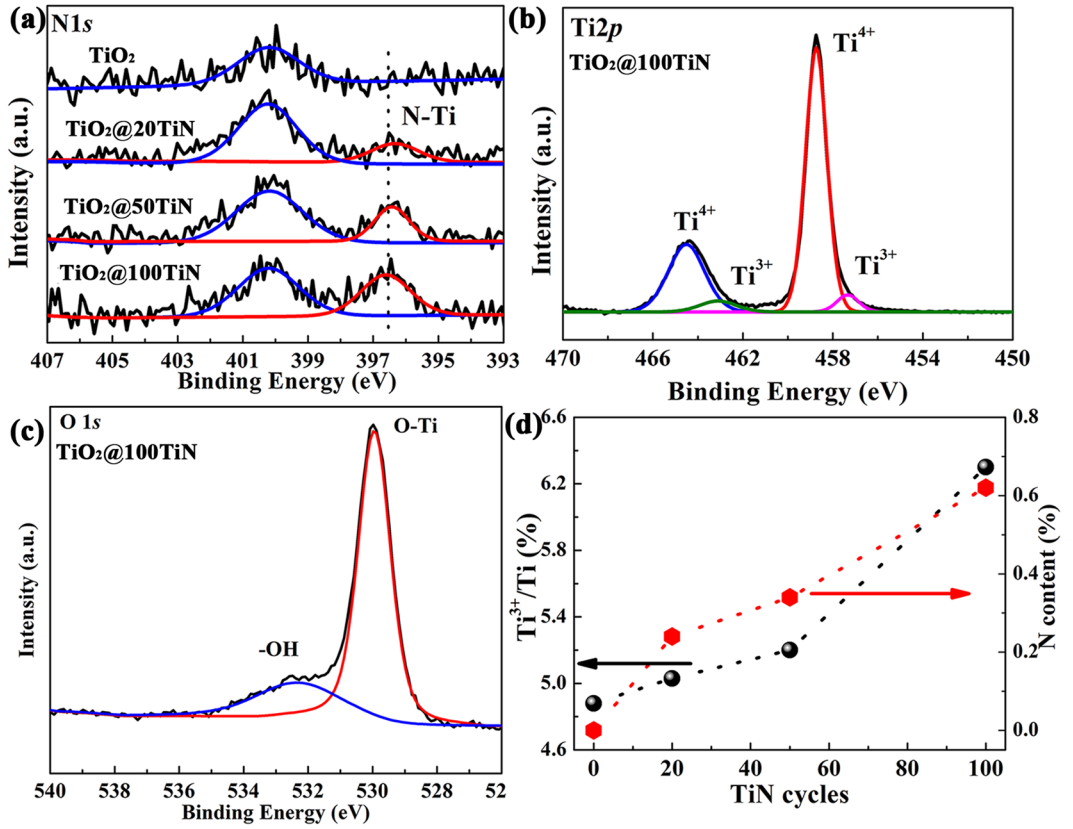

Figure 1. (**a**) N 1s XPS spectra of pristine TiO_2 and TiO_xN_y coated TiO_2 powders, (**b**) Ti 2p and (**c**) O1s spectra of TiO_2@100TiN, (**d**) Ti^{3+}/Ti ratio and N content verse TiN coating cycles.

prospects in various applications, such as lithium ion batteries[27,28], supercapacitors[29–31], catalysis[32,33], and solar energy conversions[34]. Plasma enhanced ALD (PEALD), employing plasma as one precursor, has shown some merits over conventional thermal ALD (T-ALD), such as higher film density, lower impurity, higher growth rate, better electronic properties. Moreover, less energy is required to drive the surface reaction because of the high reactivity of plasma species, resulting in a lower deposition temperature[35].

Various N-doped TiO_2 nanomaterials, which exhibit highly visible light photocatalytic performance, have been successfully synthesized. However, the effect of ultrathin N-doped TiO_2 surface coating/modification on visible light photocatalysis of TiO_2 has not been well researched. Herein, PEALD was adopted to deposit ultrathin TiN film on TiO_2 powders. The deposited TiN film would be oxidized into TiO_xN_y (N doped TiO_2) when exposed to the air, achieving TiO_xN_y coated TiO_2 after PEALD TiN coating. This ultrathin TiO_xN_y coating can facilitate the visible light absorption of TiO_2. Correspondingly, the TiO_xN_y coated TiO_2 powders exhibit significantly enhanced visible light photocatalytic activity towards methyl orange (MO) and phenol degradation.

Results

Bui *et al*. have reported that the surface of deposited TiN film would be oxidized when exposed to the air[36]. Therefore, the XPS spectra of the TiN film deposited by PEALD on silicon were firstly conducted to explore the surface chemistry of as-deposited TiN, as shown in Fig. S1. Both Ti-O and Ti-N bonding can be detected in Ti 2*p* spectra, confirming the formation of TiO_xN_y on the PEALD TiN surface, in consistent with reported literature[36]. Therefore, it can be speculated that TiO_xN_y coated TiO_2 composite can be achieved here after coating ultrathin PEALD TiN on TiO_2 surface.

Next, the surface chemical nature of PEALD TiN coated TiO_2 catalyst was also characterized by XPS. XPS spectra were fitted with Gaussian-Lorentzian (G-L) functions after smart-type background subtraction. Figure 1a shows the N 1 s spectra of pristine TiO_2 and PEALD TiN coated TiO_2. It can be found that pristine TiO_2 only exhibits a weak peak at ~400.1 eV, which can be assigned to absorptive nitrogen molecules[37,38]. After PEALD TiN coating, there appears a new peak at 396.5 eV, corresponding to the formation of N-Ti bonding[37,38]. And the intensity of N-Ti is enhanced with increasing the PEALD TiN cycles. In Ti 2p spectra of pristine TiO_2 (Fig. S2a), the doublet at 464.4 and 458.7 eV can be assigned to Ti $2p_{1/2}$ and Ti $2p_{3/2}$ peaks of Ti-O bonds with the spin orbit splitting energy of 5.7 eV, consistent with the value of TiO_2[11]. Besides, there are two weak doublet peaks at 462.9 eV and 457.2 eV can also be detected, which can be assigned to Ti^{3+} defects on the surface[39]. More Ti^{3+} can be introduced onto the surface of TiO_2 after PEALD TiN coating. Therefore, the surface Ti^{3+}/Ti ratio increases with increasing PEALD deposition cycles, as shown in Fig. 1d. All the samples show the similar O 1s spectra with main O-Ti bonds of TiO_2 at 529.9 eV, as shown in Fig. 1c and Fig. S2, the peak at 532.4 eV related to the -OH

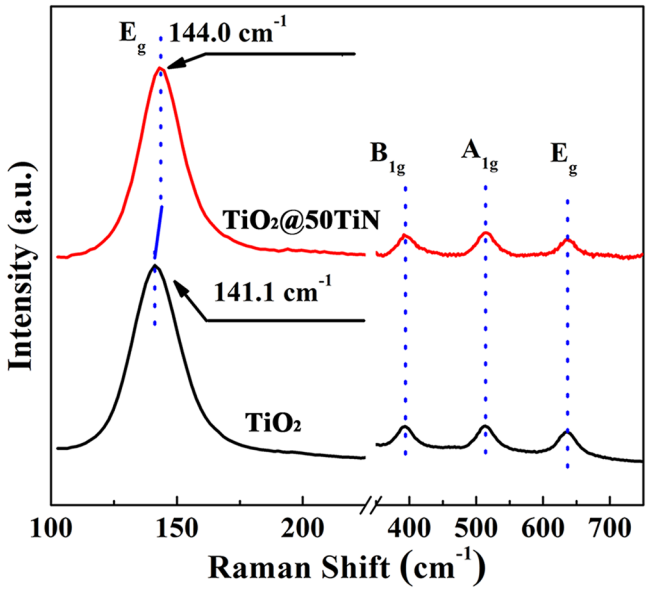

Figure 2. Raman spectra of pristine TiO_2 and TiO_2@50TiN powders.

on the surface can also be detected[7]. Figure 1d illustrates the plots of surface Ti^{3+}/Ti ratio and N content versus the PEALD TiN cycles, it can be seen that both surface Ti^{3+} and N content increase with PEALD TiN cycles. Combined with XPS data of PEALD TiN film on Si (Fig. S1), it can be concluded that TiO_xN_y coating layer was formed on TiO_2 surface after ultrathin PEALD TiN coating. It has been proved in previous literatures that both Ti^{3+} and N sites can narrow the band gap of TiO_2[40,41]. Therefore, it can be speculated that a much smaller band gap can be achieved for the TiO_xN_y layer, promoting the visible light absorption.

Figure 2 shows the Raman spectra of pristine TiO_2 and TiO_2@50TiN prepared by PEALD. According to the previously reported data[42], the anatase phase of TiO_2 has six Raman bands at 144 cm^{-1} (Eg), 197 cm^{-1} (Eg), 399 cm^{-1} (B1g), 513 cm^{-1} (A1g), 519 cm^{-1} (B1g) and 639 cm^{-1} (Eg), and the rutile phase has four Raman bands at 143 cm^{-1} (B1g), 447 cm^{-1} (Eg), 612 cm^{-1} (A1g), and 826 cm^{-1} (B2g). Both samples here present Raman spectra the same as the pure anatase phase, with no peaks related to the rutile phase. More importantly, the most remarkable feature is that the predominant peak position (Eg) undergoes a blue shift from 141.1 cm^{-1} to 144.0 cm^{-1} after TiO_xN_y modification. Previous literatures have demonstrated that the N doping in TiO_2 can result in the blue shift for Eg mode[43]. Therefore, the slight blue shift here can be ascribed to the small amount TiO_xN_y formation on the TiO_2 surface.

FESEM was performed to observe the morphology and crystal size of TiO_2 and TiO_xN_y coated TiO_2 powders, as shown in Fig. S3. It can be found that the pristine TiO_2 powders show well dispersed sphere of around 10–30 nm and aggregate together. After PEALD deposition, it can be seen that ultrathin TiO_xN_y coating has no obvious effect on the morphology and crystal size of TiO_2. All the samples exhibit the similar morphology. In order to thoroughly characterize the microstructure change of TiO_2 after surface coating, high resolution transmission electron microscopy (HRTEM) was also applied to observe the microstructure of TiO_2 and TiO_2@50TiN. It can be found that pristine TiO_2 exhibits good crystallinity with a sharp well-ordered surface (Fig. 3a). After 50 cycles TiN coating, there is an amorphous layer formed on the TiO_2 surface of ~1 nm (Fig. 3b). It is supposed to be the ultrathin TiO_xN_y coating formed after PEALD TiN deposition. Besides, both samples show a lattice spacing of 0.35 nm, which corresponds to the (101) planes of anatase TiO_2. Therefore, it can be concluded from XPS spectra, Raman spectra, and HRTEM images that an amorphous ultrathin TiO_xN_y was formed on the TiO_2 surface.

The corresponding XRD patterns of pristine TiO_2 and TiO_xN_y coated TiO_2 powders are shown in Fig. 4. All the samples exhibit the similar characteristic diffraction peaks at 25.4°, 37.9°, 48.0°, 54.1°, 63.0° etc., indicating good agreement with standard anatase TiO_2 (JCPDS No. 71-1168). Besides, there are no other peaks such as Ti-N detected in the samples. In addition, the average crystal size and lattice parameters of different samples can be determined by XRD using Scherrer equation, as listed in Table 1. It can be found that the crystal size of all the samples is estimated to be around 19 nm, in agreement with SEM images. In addition, all the samples show nearly the same lattice parameters, indicating that ultrathin TiO_xN_y surface coating does not change the crystal size and average unit cell dimension. Moreover, Nitrogen adsorption-desorption isotherms were also performed to measure the surface area of TiO_2 powders, it can be found that all the samples exhibit nearly the same BET surface area of around 113 m^2/g (Table 1 and Fig. S4).

Therefore, it can be concluded that ultrathin TiO_xN_y coating can be formed on the surface of TiO_2 powders. And this ultrathin surface coating doesn't show obvious change in the morphology, crystal size, lattice parameters, and surface area of TiO_2 nano powders. However, it can be clearly seen that there is a vivid color change of TiO_2 powders from white to yellow after ultrathin TiO_xN_y surface modification, as shown in Fig. 5a,b. Hence, UV-Vis diffuse reflectance spectra were conducted to explore the influence of ultrathin TiO_xN_y surface coating on the visible light absorption of TiO_2 powders, as shown in Fig. 5c. For comparison, the spectrum of

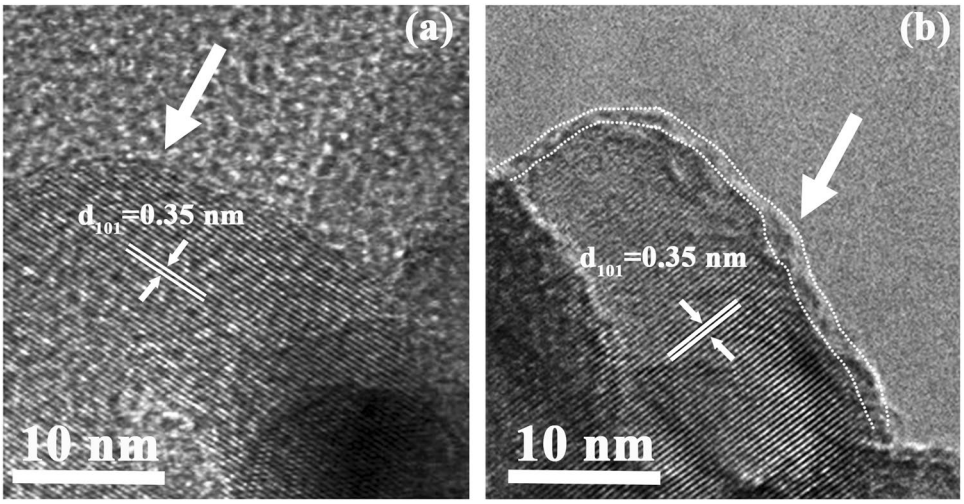

Figure 3. TEM images of (**a**) pristine TiO_2 and (**b**) TiO_xN_y coated TiO_2 (TiO_2@50TiN).

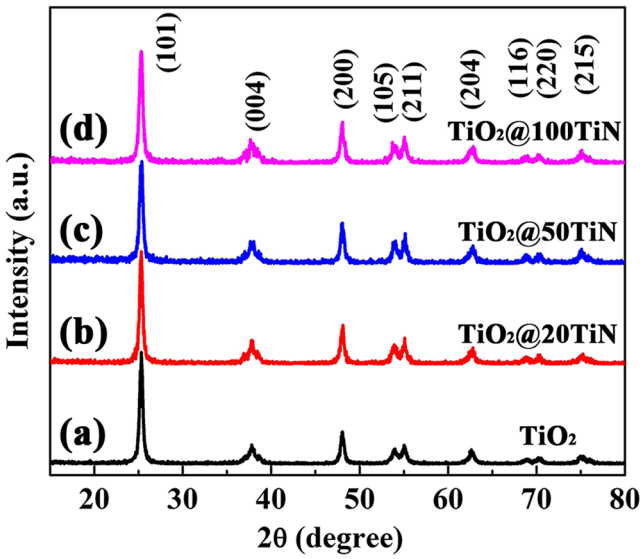

Figure 4. XRD patterns of (**a**) pristine TiO_2, (**b**) TiO_2@20TiN, (**c**) TiO_2@50TiN, and (**d**) TiO_2@100TiN.

Sample	a_0 (Å)	c_0 (Å)	Crystallite size (nm)	BET surface area (m^2/g)
TiO_2	3.78	9.54	19.03	112.6
TiO_2@20TiN	3.78	9.55	19.27	112.6
TiO_2@50TiN	3.78	9.53	18.98	111.7
TiO_2@100TiN	3.78	9.55	18.55	115.2

Table 1. Parameters of pristine TiO_2 and TiO_xN_y coated TiO_2 powders.

pristine TiO_2 powder is also illustrated. The absorption edge of pristine TiO_2 is approximately 371 nm and does not show noticeable absorption in the visible region. However, all the TiO_xN_y coated TiO_2 samples exhibit distinct and meaningful absorption in the visible range from 390 to 500 nm, consistent with previous experimental results[20,44]. Furthermore, more TiO_xN_y coating can induce more visible light absorption. For the indirect bandgap semiconductor, the relation between the absorption edge and the photon energy ($h\nu$) can be written as follows: $(\alpha h\nu)^{1/2} = A(h\nu - E_g)$, where A is the absorption constant of the indirect band gap semiconductor material. The absorption coefficient (α) is determined from the scattering and reflectance spectra according to Kubelka-Munk theory. The indirect bandgap energies estimated from the intercept of the tangents to the plots are presented in Fig. 5d. The bandgap of pristine TiO_2 powders is determined to be 3.24 eV. TiO_xN_y coated TiO_2 (100 cycles TiN) exhibits two bandgaps. The larger bandgap of 3.18 should be related to the TiO_2 supporters. Besides, a smaller

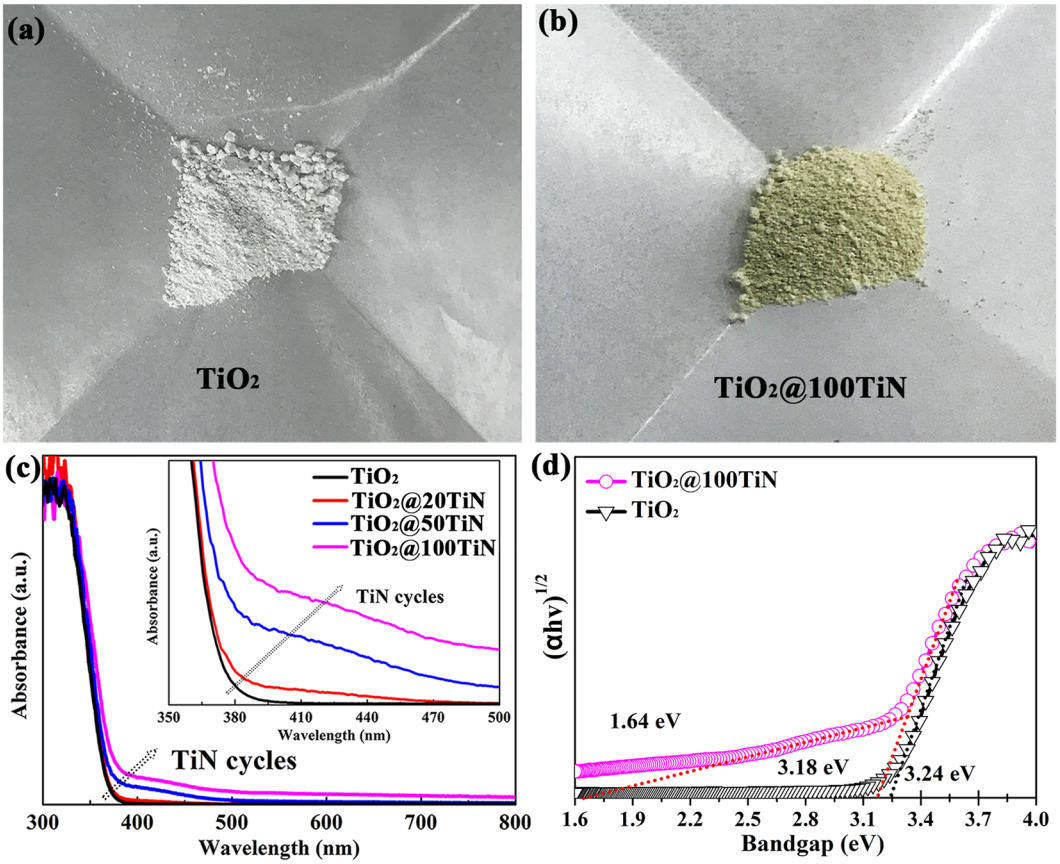

Figure 5. Optical photos of (**a**) pristine TiO_2 and (**b**) TiO_2@100TiN. (**c**) UV-Vis diffuse reflectance spectra of pristine TiO_2 and TiO_xN_y coated TiO_2 powders. (**d**) The corresponding band gaps determination plots of pristine TiO_2 and TiO_2@100TiN.

band gap of 1.64 eV can be assigned to the band gap value of TiO_xN_y coating layer. Therefore, it can be concluded that ultrathin TiO_xN_y surface modification layer with smaller band gap can facilitate the visible light absorption of TiO_2 powders.

The photocatalytic activity of TiO_xN_y coated TiO_2 has been investigated carefully through degrading methyl orange (MO) under visible light irradiation, as shown in Fig. 6. All the samples exhibit negligible adsorption capacity of MO, as shown in Fig. S5. Meanwhile, almost no degradation of MO is observed in the absence of catalyst, indicating that MO is stable under visible light irradiation. As shown in Fig. 6a, pristine TiO_2 shows very limited photocatalytic activity of ~4.4% in 120 min under visible light irradiation due to its large band gap. However, after ultrathin TiO_xN_y coating with only 20 cycles PEALD TiN, a much-improved photocatalytic activity of ~57.3% is achieved. Moreover, the photocatalytic activity improves with increasing the TiN coating cycles, with the TiO_2@100TiN exhibiting the highest degradation efficiency of ~96.5%. The experimental results were also fitted to the pseudo-first-order kinetics. At low initial pollutant concentration, the rate constant k was given by $\ln(C_t/C_0) = -kt$. Here, k and t represent the first-order rate constant (h^{-1}), and the irradiation time (h), respectively. C_0 is the initial concentration of MO, and C_t is the concentration at reaction time of t. The corresponding plots of $-\ln(C_t/C_0)$ versus the irradiation time for photodegradation of MO are shown in Fig. 6b. A linear relation between $-\ln(C_t/C_0)$ and the irradiation time has verified that the photodegradation of MO using TiO_xN_y coated TiO_2 catalyst follows the first-order kinetics. TiO_xN_y coated TiO_2 exhibit the kinetic constants of 1.62 h^{-1} (TiO_2@100 TiN), 0.82 h^{-1} (TiO_2@50 TiN), and 0.45 h^{-1} (TiO_2@20 TiN), which are much larger than pristine TiO_2 of 0.023 h^{-1}. Apparently, ultrathin TiO_xN_y coating can greatly improve the visible light photodegradation efficiency of MO due to its absorption in visible light spectrum. In order to evaluate the stability of the photocatalyst, the recycling experiments about MO photodegradation were performed with TiO_2@50TiN catalyst. As shown in Fig. 6c, the photocatalytic activity of TiO_2@50TiN exhibits an extremely limited decline for three times. The degradation efficiency of MO solution is nearly the same for three recycling experiment under 120 min irradiation, exhibiting wonderful recycling ability.

Moreover, colorless phenol was also adopted to evaluate the visible photocatalytic performance of TiO_2@50TiN. As shown in Fig. 6d, it can be seen that both pure TiO_2 and TiO_2@50TiN exhibit negligible absorption for phenol molecule in the darkness. Pure TiO_2 powder shows no photocatalytic activity towards degrading phenol molecule. There is hardly any degradation of phenol for TiO_2 with 2 h visible irradiation. However, after modification with 50 cycles of TiN, the TiO_2@50TiN powders exhibit visible photocatalytic activity for phenol,

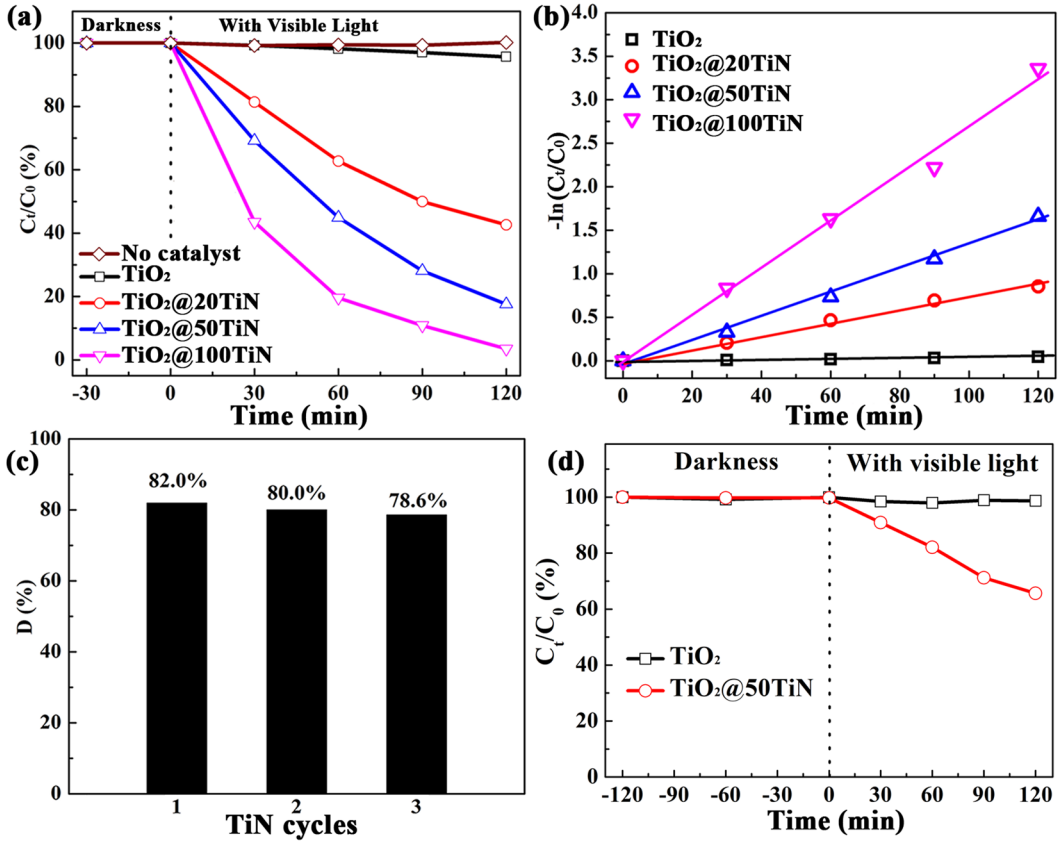

Figure 6. (**a**) Photocatalytic degradation of MO by using TiO_2 and TiO_xN_y coated TiO_2 catalysts prepared by PEALD under visible-light irradiation, (**b**) the corresponding $-\ln(C_t/C_0)$ vs. time curves, (**c**) three cycles of MO degradation for TiO_2@50TiN in 120 min, (**d**) photocatalytic degradation of phenol by using TiO_2 and TiO_2@50TiN catalysts under visible-light irradiation.

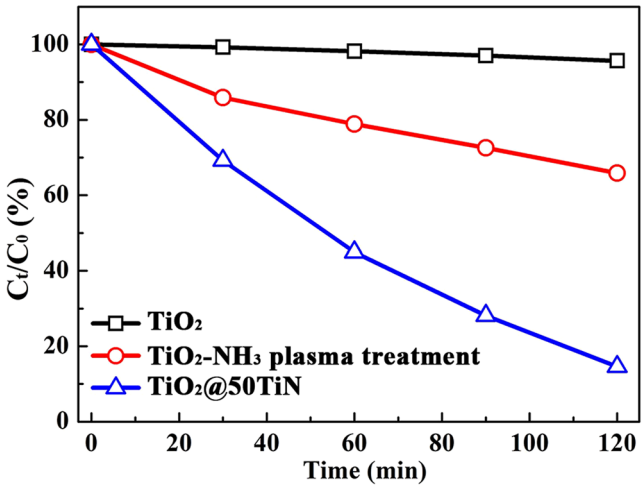

Figure 7. Photocatalytic degradation of MO by using NH_3 plasma treated TiO_2 and TiO_xN_y coated TiO_2 catalysts under visible-light irradiation.

around 34.3% of phenol can degrade in 2 h. Therefore, it can also be demonstrated that surface modification with PEALD TiN can greatly improve the visible photocatalytic activity of TiO_2.

As reported previously, visible light active photocatalytic N-doped TiO_2 can be achieved by annealing TiO_2 under NH_3 flux at high temperature[17]. Thus, a control experiment using TiO_2 photocatalyst treated by NH_3 plasma at 360 °C was also performed, as shown in Fig. 7. It can be seen that NH_3 plasma treatment can only slightly improve the photocatalytic activity of TiO_2, the photocatalytic activity is much lower than the TiO_xN_y

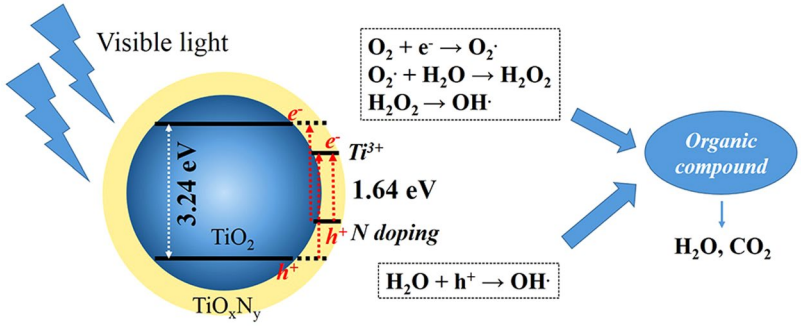

Figure 8. Proposed mechanism of TiO_xN_y coated TiO_2 for the degradation of MO under visible light irradiation.

coated sample. It can be concluded that, in order to achieve highly visible light active N-TiO_2 based photocatalyst, it is easier and more effective to coat TiO_xN_y thin film on TiO_2 than replacing O with N under NH_3 flux at high temperature.

The photocatalytic mechanism of TiO_xN_y coated TiO_2 is also proposed. There are a large number of reports focusing on the photocatalytic activity mechanism of N-doped TiO_2. It has been demonstrated that both N doping and Ti^{3+} can contribute to narrowing the band gap of TiO_2[21], the band gap alignment and charge transfer of TiO_2@TiO_xN_y is shown in Fig. 8. It is widely accepted that N doping can form a new substitution N 2p band above the O 2p valance band. While the Ti^{3+} sites exhibit the 3d orbital in the band gap, which is found to below the bottom of the conduction band[21]. Therefore, TiO_xN_y coated TiO_2 exhibits a small band gap value of ~1.64 eV here, which can absorb the visible light. Upon visible light irradiation, electrons can transfer into the conduction band of TiO_2 and Ti^{3+} sites, reducing O_2 to form O_2. radicals. The holes (h^+) formed in the valance band and N doping sites would react with H_2O to produce OH. radicals. Both radicals are responsible for the degradation of MO under visible light, as shown in Fig. 8. It should be noted that only an ultrathin TiO_xN_y coating here can significantly improve the visible light photocatalytic activity of commercial TiO_2 powders. Therefore, maybe it's needless to synthesize the monolithic N-doped TiO_2 composites, adopting ultrathin TiO_xN_y coating can be an effective approach to prepare visible light active photocatalysts. In addition, surface coating or modification using ALD technology can be easily extended to other supporters, such as porous materials, nanowires, and so on.

Conclusions

In summary, a novel and facile approach to prepare ultrathin TiO_xN_y coated TiO_2 composite by PEALD has been developed to promote the application of TiO_2 photocatalyst under visible light. An ultrathin TiO_xN_y film can be formed perfectly on the surface of TiO_2 powders using PEALD. Introducing ultrathin TiO_xN_y coating with smaller bandgap of ~1.64 eV can facilitate the absorption of TiO_2 in visible light spectrum. As a result, this ultrathin TiO_xN_y coating can extraordinarily improve the photocatalytic activity of commercials TiO_2 powders towards degrading both MO and phenol under visible light. TiO_2@100TiN prepared by PEALD photocatalyst could nearly degrade MO completely (~96.5%) in 120 min under visible light irradiation, while pristine TiO_2 shows very weak photoactivity of only 4.4%. Moreover, TiO_xN_y coated TiO_2 photocatalyst is quite stable and reusable. Therefore, this surface modification using PEALD is an extremely promising route that could also be extended to other supporters to prepare visible light active photocatalysts. These results presented in this work could open a new window to the future design and synthesis of visible light photocatalysts.

Methods

Chemicals. In ALD process, Titanium tetrachloride ($TiCl_4$) (5N, Suzhou Fornano Corporation Ltd.) and NH_3 plasma were used as Ti precursor and Nitrogen sources, respectively. High pure N_2 (5N) and Ar (5N) were used as carrier and purge gas. Commercial anatase TiO_2 powders (Nanjing Haitai nano materials Co) with diameter of ~20 nm were used as supporters. Methyl Orange (MO, $C_{14}H_{14}N_3NaO_3S$, J&K Scientific) and phenol was prepared into 4 mg L^{-1} with Milli-Q water.

Preparation of TiO_xN_y modified TiO_2 powder. TiO_2 powders were loaded into a special powder container with porous mesh. The schematic diagram of coating TiO_2 powders by PEALD TiN is shown in Fig. S6. $TiCl_4$ and NH_3 plasma were used as precursors for TiN deposition. Plasma power and NH_3 gas flow rate were 2500 W and 160 sccm, respectively. And it is a remote plasma source. Pure N_2 (5N) and Ar (5N) were used as carrier/purge gas for $TiCl_4$ and NH_3 plasma, respectively. Various cycles of TiN were deposited onto TiO_2 surface at 360 °C, where one cycle consisted of 2 s $TiCl_4$ injection, 10 s purging, 24 s NH_3 plasma injection, and 6 s purging. Long dosing/purging time was applied to gain conformal coating on nano powders. In this work, the samples coated by 20, 50, 100 cycles of TiN are termed as TiO_2@20TiN, TiO_2@50TiN and TiO_2@100TiN, respectively. As a control experiment, TiO_2 powders were treated by NH_3 plasma at 360 °C for 20 min, which is equal to the NH_3 plasma injection time of 50 cycles of PEALD TiN.

Characterization. The chemical feature was investigated by X-ray photoelectron spectroscopy (XPS, Thermo Fisher K-Alpha) with standard Al Kα (1486.7 eV) X-ray source. The binding energies were calibrated with respect

to the signal from the adventitious carbon (binding energy = 284.6 eV). Raman spectra of TiO_2 were collected by a confocal Raman microscope (LabRAM HR Evolution, Horiba) with excitation laser wavelength of 632.8 nm. An objective lens is employed to focus the excitation laser on the substrate and collect the Raman signal. The microstructure and morphology were examined by filed effect scanning electron microscopy (FESEM, Ultra55, ZEISS) and high-resolution transmission electron microscopy (HRTEM, Tecnai F20 S-Twin, FEI). Crystallinity and phase structures of powders were analyzed by a Rigaku-D/MAX 2000X-ray diffraction (XRD) system with Cu Kα radiation. The Brunauer-Emmett-Teller (BET) surface area was estimated by a surface area apparatus (TriStar-3000, Micromeritics). UV-visible absorption spectra were recorded by a UV-vis-NIR spectrophotometer (UV-3600, Shimadzu).

Photocatalytic activity. The photocatalytic activity of as-prepared photocatalysts was evaluated via the degradation of methyl orange (MO) or phenol in aqueous solution. A solar simulator (300 W Xe lamp, MircoSolar300, PerfectLight) with a 420 nm cut-off filter provides the visible-light irradiation. The lamp was located at 15 cm away from the reaction solution. 100 mg catalyst and 100 ml of aqueous solution containing 4 mg L^{-1} MO or phenol were placed in a glass reactor with continuous stirring at 500 rpm. Prior to irradiation, the pollutant solutions suspended with photocatalysts were stirred in absence of light for 30 min (MO) or 2 h (phenol) to attain the equilibrium adsorption/desorption between photocatalyst powders and organic molecules. During the reaction, the temperature was maintained at 25 ± 1 °C using cooling water. For each given irradiation time, about 3 mL of the reacted solution was withdrawn and centrifuged at 10,000 rpm for 10 min to remove the photocatalyst. Then, the concentration of the centrifuged solution was determined by a UV-vis-NIR spectrophotometer, measuring the maximum absorption of MO at 464 nm and phenol at 270 nm.

Stability test of photocatalysts. In order to evaluate the stability of the photocatalysts, a recycled usage experiment was carried out. 100 mg TiO_2@50TiN photocatalyst was suspended in a 100 mL of 4 mg L^{-1} solution of MO and irradiated under Xe lamp for 120 min. The photocatalysts were collected and washed by distilled water and ethanol, then dried in the oven at 100 °C for 12 h. Finally, the photocatalyst was reused again for the second cycle of degradation with a fresh dye solution. This process was about to repeat up to 3 times of application.

References

1. Fujishima, A. Electrochemical photolysis of water at a semiconductor electrode. *Nature* **238**, 37–38 (1972).
2. Chen, X. & Mao, S. S. Titanium dioxide nanomaterials: synthesis, properties, modifications, and applications. *Chem. Rev* **107**, 2891–2959 (2007).
3. Pelaez, M. *et al*. A review on the visible light active titanium dioxide photocatalysts for environmental applications. *Appl. Catal. B Environ.* **125**, 331–349 (2012).
4. Linsebigler, A. L., Lu, G. & Yates, J. T. Jr. Photocatalysis on TiO_2 surfaces: principles, mechanisms, and selected results. *Chem. Rev* **95**, 735–758 (1995).
5. Ohno, T., Mitsui, T. & Matsumura, M. Photocatalytic activity of S-doped TiO_2 photocatalyst under visible light. *Chem. Lett* **32**, 364–365 (2003).
6. Diwald, O. *et al*. Photochemical activity of nitrogen-doped rutile TiO_2 (110) in visible light. *J. Phys. Chem. B* **108**, 6004–6008 (2004).
7. Yan, X. *et al*. The interplay of sulfur doping and surface hydroxyl in band gap engineering: Mesoporous sulfur-doped TiO_2 coupled with magnetite as a recyclable, efficient, visible light active photocatalyst for water purification. *Appl. Catal. B Environ* **218**, 20–31 (2017).
8. Zhang, Z., Zhang, L., Hedhili, M. N., Zhang, H. & Wang, P. Plasmonic gold nanocrystals coupled with photonic crystal seamlessly on TiO_2 nanotube photoelectrodes for efficient visible light photoelectrochemical water splitting. *Nano Lett* **13**, 14–20 (2012).
9. Li, G.-S., Zhang, D.-Q. & Yu, J. C. A new visible-light photocatalyst: CdS quantum dots embedded mesoporous TiO_2. *Environ. Sci. Technol* **43**, 7079–7085 (2009).
10. Choi, T., Kim, J.-S. & Kim, J. H. Transparent nitrogen doped TiO_2/WO_3 composite films for self-cleaning glass applications with improved photodegradation activity. *Adv. Powder Technol* **27**, 347–353 (2016).
11. Guo, X. *et al*. Porous TiB_2-TiC/TiO_2 heterostructures: Synthesis and enhanced photocatalytic properties from nanosheets to sweetened rolls. *Appl. Catal. B Environ* **217**, 12–20 (2017).
12. Fujishima, A., Zhang, X. & Tryk, D. A. TiO_2 photocatalysis and related surface phenomena. *Surf. Sci. Rep* **63**, 515–582 (2008).
13. Zhang, J., Wu, Y., Xing, M., Leghari, S. A. K. & Sajjad, S. Development of modified N doped TiO_2 photocatalyst with metals, nonmetals and metal oxides. *Energ. Environ. Sci* **3**, 715–726 (2010).
14. Burda, C. *et al*. Enhanced nitrogen doping in TiO_2 nanoparticles. *Nano Lett* **3**, 1049–1051 (2003).
15. Chen, X., Lou, Y. B., Samia, A. C., Burda, C. & Gole, J. L. Formation of Oxynitride as the Photocatalytic Enhancing Site in Nitrogen-Doped Titania Nanocatalysts: Comparison to a Commercial Nanopowder. *Adv. Funct. Mater* **15**, 41–49 (2005).
16. Shifu, C., Lei, C., Shen, G. & Gengyu, C. The preparation of nitrogen-doped photocatalyst $TiO_{2-x}N_x$ by ball milling. *Chem. Phys. Lett* **413**, 404–409 (2005).
17. Lai, Y.-K. *et al*. Nitrogen-doped TiO_2 nanotube array films with enhanced photocatalytic activity under various light sources. *J. Hazard. Mater* **184**, 855–863 (2010).
18. Martínez-Ferrero, E. *et al*. Nanostructured Titanium Oxynitride Porous Thin Films as Efficient Visible-Active Photocatalysts. *Adv. Funct. Mater* **17**, 3348–3354 (2007).
19. Quesada-Cabrera, R. *et al*. On the apparent visible-light and enhanced UV-light photocatalytic activity of nitrogen-doped TiO_2 thin films. *J. Photochem. Photobio. A Chem* **333**, 49–55 (2017).
20. Lee, A. *et al*. Conformal Nitrogen-Doped TiO_2 Photocatalytic Coatings for Sunlight-Activated Membranes. *Adv. Sustainable Sys.* **1**, 1600041 (2017).
21. Yang, G., Jiang, Z., Shi, H., Xiao, T. & Yan, Z. Preparation of highly visible-light active N-doped TiO_2 photocatalyst. *J. Mater. Chem* **20**, 5301–5309 (2010).
22. Luong, N. S. *et al*. Highly Visible Light Activity of Nitrogen Doped TiO_2 Prepared by Sol-Gel Approach. *J. Electron. Mater* **46**, 158–166 (2017).
23. Liu, M., Li, X., Karuturi, S. K., Tok, A. I. Y. & Fan, H. J. Atomic layer deposition for nanofabrication and interface engineering. *Nanoscale* **4**, 1522–1528 (2012).
24. Knez, M., Nielsch, K. & Niinistö, L. Synthesis and surface engineering of complex nanostructures by atomic layer deposition. *Adv. Mater* **19**, 3425–3438 (2007).
25. Meng, X. *et al*. Atomic Layer Deposition for Nanomaterials Synthesis and Functionalization in EnergyTechnology. *Mater. Horiz.* **4**, 133–154 (2017).

26. Cao, Y.-Q. *et al*. Atomic-Layer-Deposition Assisted Formation of Wafer-Scale Double-Layer Metal Nanoparticles with Tunable Nanogap for Surface-Enhanced Raman Scattering. *Sci. Rep* **7**, 5161 (2017).
27. Meng, X., Yang, X.-Q. & Sun, X. Emerging Applications of Atomic Layer Deposition for Lithium-Ion Battery Studies. *Adv. Mater* **24**, 3589–3615 (2012).
28. Cao, Y., Meng, X. & Elam, J. W. Atomic Layer Deposition of Li_xAl_yS Solid-State Electrolytes for Stabilizing Lithium-Metal Anodes. *Chem Electro Chem* **3**, 858–863 (2016).
29. Guan, C. & Wang, J. Recent Development of Advanced Electrode Materials by Atomic Layer Deposition for Electrochemical Energy Storage. *Adv. Sci* **3**, 1500405 (2016).
30. Ahmed, B., Xia, C. & Alshareef, H. N. Electrode surface engineering by atomic layer deposition: A promising pathway toward better energy storage. *Nano Today* **11**, 250–271 (2016).
31. Cao, Y.-Q. *et al*. ZnO/ZnS Core-Shell Nanowires Arrays on Ni Foam Prepared by Atomic Layer Deposition for High Performance Supercapacitors. *J. Electrochem. Soc* **164**, A3493–A3498 (2017).
32. Lu, J., Elam, J. W. & Stair, P. C. Atomic layer deposition-Sequential self-limiting surface reactions for advanced catalyst "bottom-up" synthesis. *Surf. Sci. Rep* **71**, 410–472 (2016).
33. Cao, Y. Q. *et al*. Photocatalytic activity and photocorrosion of atomic layer deposited ZnO ultrathin films for the degradation of methylene blue. *Nanotechnology* **26**, 024002 (2015).
34. Wang, T., Luo, Z., Li, C. & Gong, J. Controllable fabrication of nanostructured materials for photoelectrochemical water splitting via atomic layer deposition. *Chem. Soc. Rev* **43**, 7469–7484 (2014).
35. Profijt, H., Potts, S., Van de Sanden, M. & Kessels, W. Plasma-assisted atomic layer deposition: Basics, opportunities, and challenges. *J. Vac. Sci. Technol. A* **29**, 050801 (2011).
36. Van Bui, H. *et al*. Growth kinetics and oxidation mechanism of ALD TiN thin films monitored by *in situ* spectroscopic ellipsometry. *J. Electrochem. Soc* **158**, H214–H220 (2011).
37. Saha, N. C. & Tompkins, H. G. Titanium nitride oxidation chemistry: An X-ray photoelectron spectroscopy study. *J. Appl. Phys* **72**, 3072–3079 (1992).
38. Asahi, R., Morikawa, T., Ohwaki, T., Aoki, K. & Taga, Y. Visible-light photocatalysis in nitrogen-doped titanium oxides. *Science* **293**, 269–271 (2001).
39. Shultz, A. N. *et al*. Comparative second harmonic generation and X-ray photoelectron spectroscopy studies of the UV creation and O_2 healing of Ti^{3+} defects on (110) rutile TiO_2 surfaces. *Surf. Sci* **339**, 114–124 (1995).
40. Chen, Y. *et al*. Microwave-assisted ionic liquid synthesis of Ti^{3+} self-doped TiO_2 hollow nanocrystals with enhanced visible-light photoactivity. *Appl. Catal. B Environ* **191**, 94–105 (2016).
41. Livraghi, S. *et al*. Origin of photoactivity of nitrogen-doped titanium dioxide under visible light. *J. Am. Chem. Soc* **128**, 15666–15671 (2006).
42. Yanagisawa, K. & Ovenstone, J. Crystallization of anatase from amorphous titania using the hydrothermal technique: effects of starting material and temperature. *J. Phys. Chem. B* **103**, 7781–7787 (1999).
43. Wang, J., Zhu, W., Zhang, Y. & Liu, S. An efficient two-step technique for nitrogen-doped titanium dioxide synthesizing: visible-light-induced photodecomposition of methylene blue. *J. Phys. Chem. C* **111**, 1010–1014 (2007).
44. Irie, H., Watanabe, Y. & Hashimoto, K. Nitrogen-concentration dependence on photocatalytic activity of $TiO_{2-x}N_x$ powders. *J. Phys. Chem. B* **107**, 5483–5486 (2003).

Acknowledgements

This work is supported by the Natural Science Foundation of China and Jiangsu Province (51571111, BK2016230, and BK20170645), a grant from the State Key Program for Basic Research of China (2015CB921203). Dr. Yan-Qiang Cao also thanks the support from the general grant from the China Postdoctoral Science Foundation (2017M611778) and the Fundamental Research Funds for the Central Universities (021314380075).

Author Contributions

Y.Q.C. and J.C. prepared samples, and X.R.Z. and J.C. performed the photocatalytic experiments. W.Z. conducted XPS analysis. Y.Q.C. and X.J.Z. performed Raman detection. X.R.Z. conducted the TEM characterization. L.Z. and M.L. performed the SEM observations. Y.Q.C. prepared the manuscript. X.J.Z., A.D.L. and D.W. contributed to the discussion and analysis of the results. All the authors reviewed the manuscript.

Additional Information

Supplementary information accompanies this paper at https://doi.org/10.1038/s41598-018-30726-w.

Competing Interests: The authors declare no competing interests.

Publisher's note: Springer Nature remains neutral with regard to jurisdictional claims in published maps and institutional affiliations.

Open Access This article is licensed under a Creative Commons Attribution 4.0 International License, which permits use, sharing, adaptation, distribution and reproduction in any medium or format, as long as you give appropriate credit to the original author(s) and the source, provide a link to the Creative Commons license, and indicate if changes were made. The images or other third party material in this article are included in the article's Creative Commons license, unless indicated otherwise in a credit line to the material. If material is not included in the article's Creative Commons license and your intended use is not permitted by statutory regulation or exceeds the permitted use, you will need to obtain permission directly from the copyright holder. To view a copy of this license, visit http://creativecommons.org/licenses/by/4.0/.

© The Author(s) 2018